International Journal of Thermal Sciences 49 (2010) 931–940

Contents lists available at ScienceDirect

International Journal of Thermal Sciences

journal homepage: www.elsevier.com/locate/ijts

Brownian motion of nanoparticles in a triangular enclosure with natural convection

B. Ghasemi [a,*], S.M. Aminossadati [b]

[a] Shahrekord University, Faculty of Engineering, P.O. Box 115, Shahrekord, Iran
[b] The University of Queensland, School of Mechanical and Mining Engineering, QLD 4072, Australia

ARTICLE INFO

Article history:
Received 20 August 2009
Received in revised form
22 November 2009
Accepted 25 December 2009
Available online 10 February 2010

Keywords:
Triangular enclosure
Natural convection
Nanofluid
Brownian motion

ABSTRACT

This paper presents the results of a numerical study on the natural convection in a right triangular enclosure, with a heat source on its vertical wall and filled with a water–CuO nanofluid. The effects of parameters such as Rayleigh number, solid volume fraction, heat source location, enclosure aspect ratio and Brownian motion on the flow and temperature fields as well as the heat transfer rate, are examined. The results show that when Brownian motion is considered in the analysis, the solid volume fraction, the heat source location and the enclosure aspect ratio affect the heat transfer performance differently at low and high Rayleigh numbers. At high Rayleigh numbers, an optimum value for the solid volume fraction is found which results in the maximum heat transfer rate. This is in contradiction to the results of the analysis in which Brownian motion is neglected.

1. Introduction

Natural convection in triangular enclosures has been a subject of interest in many research studies because of its applicability in various fields such as air-filled attic spaces of sloped-roof-buildings [1,2], roof type solar stills [3], triangular shaped solar collectors [4–6] and miniaturised electronic components [7,8]. For the first time, Flack et al. [9] experimentally studied natural convection in an isosceles air-filled triangular enclosure with two isothermal walls and an insulated bottom. Since then, comprehensive numerical and experimental studies have been conducted on natural convection in triangular enclosures. The numerical studies on natural convection in air-filled triangular enclosures aimed to investigate the effects of pertinent parameters such as the geometry of triangular enclosure, the thermal boundary conditions, and the buoyancy effects on the thermal performance of the enclosure [10–15]. In addition to numerical studies, some researchers have experimentally studied natural convection in triangular enclosures. For example, Flack et al. [16] obtained laser velocimetry data to determine the flow velocity in a triangular enclosure and compared the results against the theoretical simulations.

Previous studies on natural convection in triangular enclosures have considered a base fluid with a low thermal conductivity. This, in turn, limits the enhancement of heat transfer in the enclosure. In some applications, such as miniaturised electronic devices, it is required to remove a significant amount of generated heat from the system through very small surfaces. Therefore, an enhanced heat transfer technique should be utilised to maintain the temperature of electronic components below safe limits. An enhanced heat transfer can be achieved by introducing high thermal conductivity nanoparticles into the base fluid within the enclosure [17]. Conceptually, it is expected that the presence of the nanoparticles in the nanofluid increases the thermal conductivity and therefore substantially enhances the heat transfer characteristics of the nanofluid.

It must also be noted that the heat transfer enhancement by means of nanofluids is still a controversial subject and there are contradictory studies reported in the literature that show that the dispersion of nanoparticles in the base fluid may result in a considerable decrease in the heat transfer [18,19]. It has been demonstrated that the augmentation or mitigation of the heat transfer found in the numerical studies depends on the existing models used to predict the properties of nanofluids [20]. Abu-Nada [21] implemented new models for nanofluids properties and examined the heat transfer enhancement under a wide range of temperatures and solid volume fractions. He argued that the heat transfer enhancement depends on the nanofluid viscosity and thermal conductivity models, and the range of Rayleigh numbers and solid volume fractions.

Recently, many theoretical studies have been carried out and several models have been proposed to predict the effective thermal

* Corresponding author. Tel./fax: +98 381 4424438.
E-mail addresses: behzadgh@yahoo.com, ghasemi@eng.sku.ac.ir (B. Ghasemi).

1290-0729/$ – see front matter © 2010 Elsevier Masson SAS. All rights reserved.
doi:10.1016/j.ijthermalsci.2009.12.017

Nomenclature

AR	enclosure aspect ratio (H/L)
C_p	specific heat, J kg^{-1} K^{-1}
d	distance of the heat source from the horizontal wall, m
D	dimensionless distance of the heat source from the horizontal wall (d/L)
g	gravitational acceleration, m s^{-2}
H	length of vertical wall of the enclosure, m
k	thermal conductivity, W m^{-1} K^{-1}
L	length of horizontal wall of the enclosure, m
Nu	local Nusselt number on the heat source
Nu_m	average Nusselt number
p	fluid pressure, Pa
$\overline{p}$	modified pressure ($p+\rho_c g y$)
P	dimensionless pressure ($\overline{p}L^2/\rho_{nf}\alpha_f^2$)
Pr	Prandtl number (ν_f/α_f)
R_{np}	radius of nanoparticles, m
Ra	Rayleigh number ($g\beta_f L^3(T_h-T_c)/\nu_f\alpha_f$)
S_φ	source term in Eq. (1)
T	temperature, K
u,v	velocity components in x,y directions, m s^{-1}
U,V	dimensionless velocity components ($uL/\alpha_f, vL/\alpha_f$)
w	heat source length, m
W	dimensionless heat source length (w/L)
x,y	Cartesian coordinates, m
X,Y	dimensionless coordinates ($x/L, y/L$)

Greek symbols

α	thermal diffusivity, m^2 s^{-1}
β	thermal expansion coefficient, K^{-1}
ϕ	solid volume fraction
Γ_φ	diffusion term in Eq. (1)
φ	non-dimensional parameter in Eq. (1)
κ	Boltzmann constant, J K^{-1}
μ	Dynamic viscosity, N s m^{-2}
ν	kinematic viscosity, m^2 s^{-1}
θ	dimensionless temperature $(T-T_c)/(T_h-T_c)$
ρ	density, kg m^{-3}
ψ_{max}	maximum stream function

Subscripts

c	cold wall
eff	effective
f	fluid (pure)
h	heat source
nf	nanofluid
np	nanoparticle

conductivity of nanofluids. In order to consider the movement of nanoparticles, some researchers have included the contribution of a dynamic component related to particle Brownian motions in their model development [22–27]. However, there is still a debate on the appropriate modelling of Brownian motion of nanoparticles and most of the research studies on nanofluids still rely on either original or modified models proposed by Maxwell [28] and Hamilton-Crosser [29], which consider the nanoparticles to be surrounded by an interfacial layer, instead of utilising bare nanoparticles.

The present study has been motivated by the need to determine the detailed flow field, temperature distribution and natural convection heat transfer in a triangular enclosure filled with a nanofluid, where Brownian motion is taken into consideration. To the best knowledge of the authors, no study which considers this problem has yet been reported in the literature. As such, the focus of this paper is to examine the effects of pertinent parameters such as Rayleigh number, solid volume fraction, heat source position, enclosure aspect ratio and Brownian motion on the natural convection characteristics of a triangular enclosure filled with a water–CuO nanofluid.

2. Problem description

A schematic diagram of the physical domain and the grid distribution considered for the physical domain are shown in Fig. 1a and b, respectively. The model consists of a right triangular enclosure with a vertical wall of length H and a horizontal wall of length L. The horizontal and vertical walls of the enclosure are thermally insulated, and the inclined wall is maintained at a relatively low temperature of T_c. A heat source with a uniform temperature of T_h and a length of w is located on the vertical wall of the enclosure. It is assumed that the enclosure is filled with a water–CuO nanofluid, water and CuO nanoparticles are in thermal equilibrium, the nanofluid is Newtonian and incompressible, the flow is laminar and radiation effects are negligible. The CuO nanoparticles are assumed to be spherical with a radius of $R_{np} = 10$ nm. Constant thermophysical properties are considered for the nanofluid, except for the density variation in the buoyancy forces, determined by using the Boussinesq approximation. The thermophysical properties of water and CuO are given in Table 1.

3. Governing equations

The equations that govern the conservation of mass, momentum and energy can be written in a non-dimensional form as shown in Eq. (1).

$$\frac{\partial(U\varphi)}{\partial X}+\frac{\partial(V\varphi)}{\partial Y}=\frac{\partial}{\partial X}\left(\Gamma_\varphi\frac{\partial\varphi}{\partial X}\right)+\frac{\partial}{\partial Y}\left(\Gamma_\varphi\frac{\partial\varphi}{\partial Y}\right)+S_\varphi \tag{1}$$

where, φ stands for the dependent non-dimensional parameters U, V and θ, and Γ_φ and S_φ are the corresponding diffusion and source terms, respectively, as summarised in Table 2. In this table, the effective density of the nanofluid is

$$\rho_{nf} = (1-\phi)\rho_f+\phi\rho_{np} \tag{2}$$

where, ϕ is the solid volume fraction of the nanofluid. The thermal diffusivity of the nanofluid is

$$\alpha_{nf} = k_{eff}/(\rho C_p)_{nf} \tag{3}$$

where $(\rho C_p)_{nf}$ is the heat capacitance of the nanofluid and is given by

$$(\rho C_p)_{nf} = (1-\phi)(\rho C_p)_f+\phi(\rho C_p)_{np} \tag{4}$$

The thermal expansion coefficient of the nanofluid is

$$(\rho\beta)_{nf} = (1-\phi)(\rho\beta)_f+\phi(\rho\beta)_{np} \tag{5}$$

The effective viscosity (μ_{eff}) and the effective thermal conductivity (k_{eff}) of the nanofluid are determined based on the models presented in Table 3. The non-dimensional groups presented in Eq. (6) are used in the present analysis.

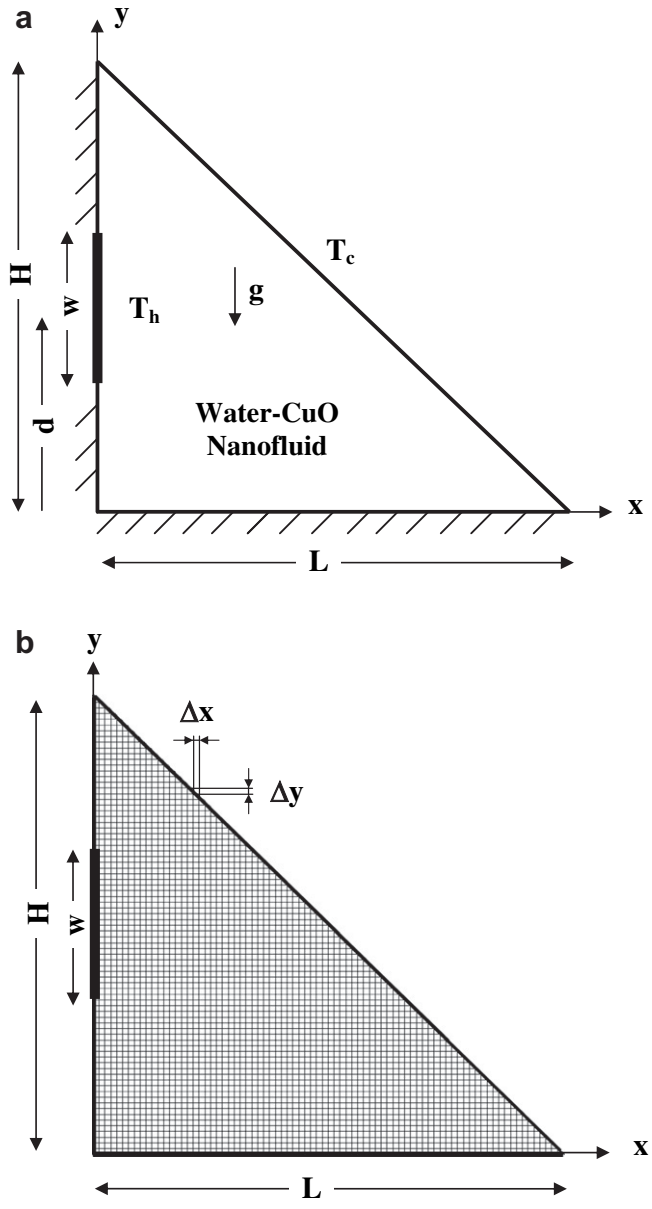

Fig. 1. a: A schematic diagram of the physical domain. b: Grid distribution considered for the physical domain.

$$X = \frac{x}{L}, \quad Y = \frac{y}{L}, \quad U = \frac{uL}{\alpha_f}, \quad V = \frac{vL}{\alpha_f}, \quad P = \frac{\overline{p}L^2}{\rho_{nf}\alpha_f^2}$$
$$\theta = \frac{T - T_c}{T_h - T_c}, \quad Ra = \frac{g\beta_f L^3 (T_h - T_c)}{\nu_f \alpha_f}, \quad \Pr = \frac{\nu_f}{\alpha_f} \tag{6}$$

Table 1
Physical properties of pure water and CuO [35].

	ρ (kg m^{-3})	C_p (J kg^{-1} K^{-1})	k (Wm^{-1} K^{-1})	β (K^{-1})
Pure water	997.1	4179	0.613	2.1×10^{-4}
CuO	6320	531.8	76.5	1.8×10^{-5}

Table 2
A summary of the governing non-dimensional equations.

Equations	φ	Γ_φ	S_φ
Continuity	1	0	0
X-momentum	U	$\mu_{eff}/\rho_{nf}\alpha_f$	$-\partial P/\partial X$
Y-momentum	V	$\mu_{eff}/\rho_{nf}\alpha_f$	$-\partial P/\partial Y + ((\rho\beta)_{nf}/(\rho_{nf}\beta_f))Ra\Pr\theta$
Energy	θ	α_{nf}/α_f	0

The non-dimensional boundary conditions are as follows:

- Along all the walls of the enclosure $U = V = 0$
- Along the heat source on the vertical wall of the enclosure $\theta = 1$
- Along the insulated vertical wall of the enclosure $\partial\theta/\partial X = 0$
- Along the horizontal wall of the enclosure $\partial\theta/\partial Y = 0$
- Along the inclined wall of the enclosure $\theta = 0$

(7)

4. Numerical approach

The control volume formulation given by Patankar [30] and the SIMPLE algorithm are utilised to solve the governing Eq. (1) with the corresponding boundary conditions given in Eq. (7). The convection–diffusion terms are discretized by a power-law scheme and the system is numerically modelled in FORTRAN. In this study, a regular rectangular domain with a uniform grid is used. The inclined wall of the enclosure is approximated with stair case-like zigzag lines and the grid cells outside of the triangular domain are assumed inactive. This method has been well documented in the literature and applied in the research studies by Asan and Namli [2] and Varol et al. [31].

After solving the governing equations for U, V and θ, other useful quantities such as Nusselt number can be determined. The local Nusselt number on the heat source surface can be defined as:

$$Nu = -\frac{k_{eff}}{k_f}\left(\frac{\partial\theta}{\partial X}\right)_{\text{on the heater}} \tag{8}$$

The average Nusselt number is determined by integrating the local Nusselt number along the heat source:

$$Nu_m = \frac{1}{W}\int_{\text{along the heater}} Nu \cdot dY \tag{9}$$

5. Grid independency and code validation

A grid independency study has been carried out for $D = 0.5$, $Ra = 10^5$, $\phi = 0.04$ and AR = 1. Fig. 2 presents the average Nusselt number (Nu_m) and maximum stream function ($|\psi_{max}|$) for five different grid sizes. A grid size of 80 × 80 is found to meet the requirements of both the grid independency study and the computational time limits. The convergence criteria are to reduce the maximum mass residual of the grid control volume below 10^{-8}.

The present computation is validated against the results of Akinsete and Coleman [1], Asan and Namli [2], Varol et al. [31] and Tzeng et al. [32] (Fig. 3a). A triangular enclosure with AR = 0.25 and filled with air ($Pr = 0.73$, $Ra = 2772$) is considered. This enclosure has a thermally insulated vertical wall, a horizontal wall at T_h and an inclined wall at T_c. It is found that the present results compare very well with other reported values. The present work is also validated against the results of Oztop and Abu-Nada [33] for a square enclosure filled with water–Cu nanofluid. A heat source with a uniform temperature (T_h) is considered on the left wall of the enclosure, the right wall is maintained at a relatively low temperature (T_c) and the other walls are thermally insulated. Fig. 3b shows the variation of Nu_m with respect to solid volume fraction (ϕ) for

Table 3
Applied models for the effective viscosity and thermal conductivity of nanofluid.

Properties	Applied model
Effective viscosity	$\mu_{eff} = \mu_{Static} + \mu_{Brownian}$
Static viscosity [36]	$\mu_{Static} = \mu_f/(1-\phi)^{2.5}$
Brownian viscosity [37]	$\mu_{Brownian} = 5\times10^4\beta\phi\rho_f\sqrt{\frac{\kappa T}{2\rho_{np}R_{np}}}f(T,\phi)$
Effective Thermal conductivity	$k_{eff} = k_{Static} + k_{Brownian}$
Static thermal conductivity [28,33,38,39]	$k_{Static} = k_f\left[\frac{(k_{np}+2k_f)-2\phi(k_f-k_{np})}{(k_{np}+2k_f)+\phi(k_f-k_{np})}\right]$
Brownian thermal conductivity [25]	$k_{Brownian} = 5\times10^4\beta\phi\rho_f C_{p,f}\sqrt{\frac{\kappa T}{2\rho_{np}R_{np}}}f(T,\phi)$
Boltzmann constant [25]	$\kappa = 1.3807\times10^{-23}$ J/K
Modelling function,β [25]	$\beta = 0.0137(100\phi)^{-0.8229}$ for $\phi < 1\%$ $\beta = 0.0011(100\phi)^{-0.7272}$ for $\phi > 1\%$
Modelling function,$f(T,\phi)$ [25]	$f(T,\phi) = (-6.04\phi + 0.4705)T + (1722.3\phi - 134.63)$ for $1\% \le \phi \le 4\%$ and $300\,K < T < 325\,K$

three different values of Rayleigh numbers ($Ra = 10^3$, 10^4 and 10^5). It can be seen that the results agree well with the results reported in the literature.

6. Results

The constant properties considered in the computation are as follows: The length of the heat source ($W = w/L$) is 0.3, the temperature of the cold wall (T_c) is 300 K, the Prandtl number (Pr) is 6.2, the length of the horizontal wall (L) is 5 cm and the radius of spherical nanoparticles (R_{np}) is 10 nm.

6.1. Rayleigh number and solid volume fraction

For this part of the analysis, the heat source is considered to be in the middle of the vertical wall of the triangular enclosure ($D = d/L = 0.5$). The other constant values are: $AR = H/L = 1$, $10^3 \le Ra \le 10^6$ and $0.01 \le \phi \le 0.04$. Fig. 4 shows the streamlines (top) and isotherms (bottom) for the enclosure filled with water–CuO nanofluid, $\phi = 0.04$ (——) and pure water (– – –). The results are presented for four different Rayleigh numbers ranging from 10^3 to 10^6. For all Rayleigh numbers, a clock-wise single circulation cell appears within the enclosure. At low Rayleigh numbers, the absolute values of maximum stream function for both pure water and the nanofluid are low, with the isotherms distributed in the whole enclosure, rather than being parallel to the heat source. This shows that conduction dominates the heat transfer process at low Rayleigh numbers. As the Rayleigh number increases, the absolute

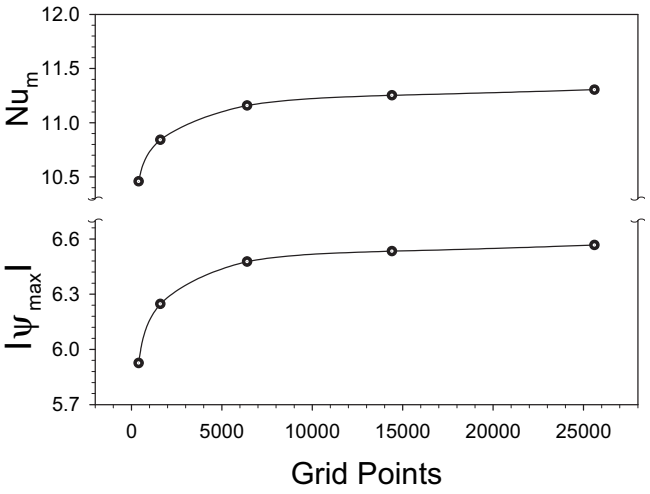

Fig. 2. Grid independency study ($Ra = 10^5$, AR = 1, $\phi = 0.04$, $D = 0.5$).

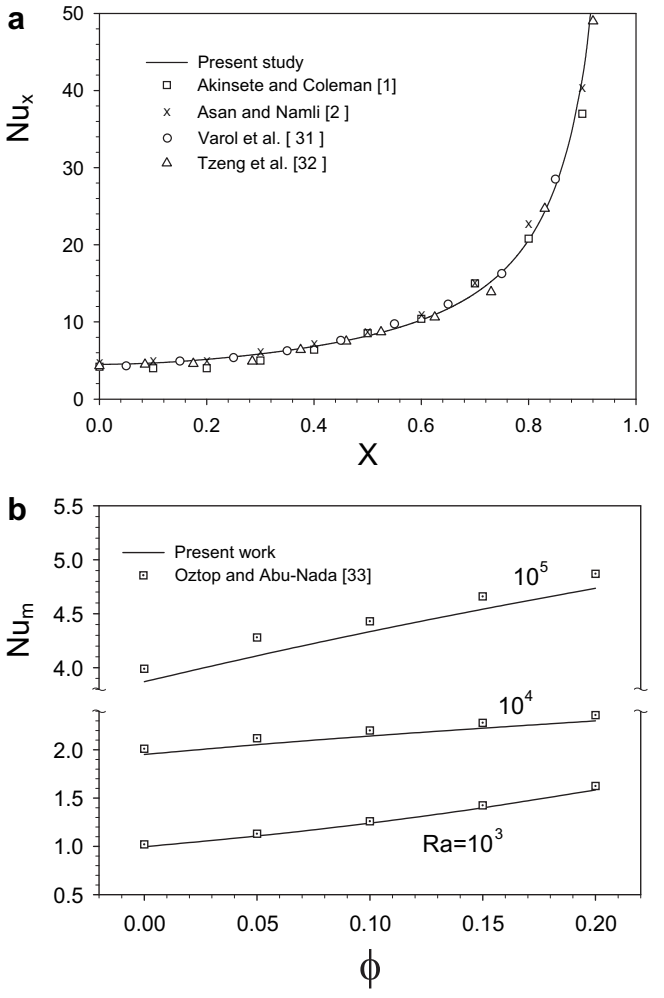

Fig. 3. a: Validation of the present code against other studies [1,2,31,32] for a triangular enclosure filled with air ($Pr = 0.73$, $Ra = 2772$, AR = 0.25). b: Validation of the present code against Oztop and Abu-Nada [33] for a square enclosure filled with a water–Cu nanofluid.

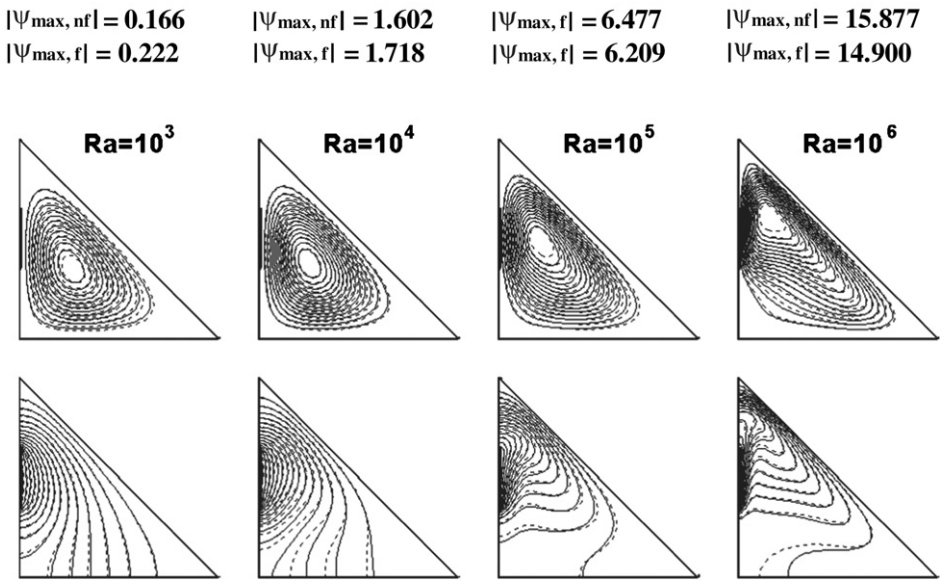

Fig. 4. Streamlines (top) and isotherms (bottom) at different Rayleigh numbers (—: nanofluid with $\phi = 0.04$ and ———: pure water).

value of the maximum stream function increases, and the centre of the circulation cell moves upwards in the enclosure. In addition, the isotherms become approximately horizontal in the middle of the enclosure, as well as stratified near the top of the enclosure and close to the heat source. This is an indication of the strengthening of the buoyancy forces at higher Rayleigh numbers.

In order to obtain a better understanding of the flow behaviour and temperature distribution within the enclosure, the *y*-velocity (V) and temperature (θ) at $Y = 0.5$ are plotted in Fig. 5a and b, respectively ($\phi = 0.04$ and $10^3 \leq Ra \leq 10^6$). Both graphs demonstrate that the absolute magnitude of V and the slope of the temperature profiles increase as the Rayleigh number increases.

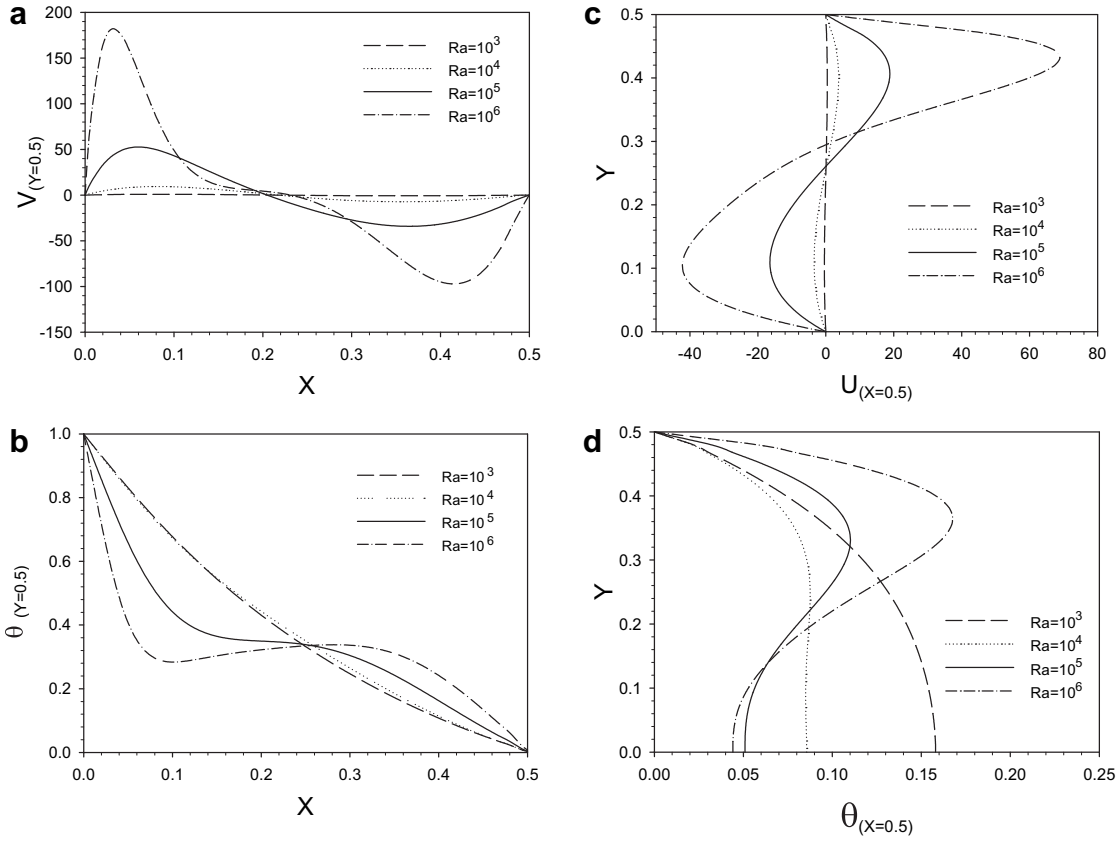

Fig. 5. a: Variation of *y*-velocity (V) at $Y = 0.5$ for different Rayleigh numbers ($\phi = 0.04$). b: Variation of temperature (θ) at $Y = 0.5$ for different Rayleigh numbers ($\phi = 0.04$). c: Variation of *x*-velocity (U) at $X = 0.5$ for different Rayleigh numbers ($\phi = 0.04$). d: Variation of temperature (θ) at $X = 0.5$ for different Rayleigh numbers ($\phi = 0.04$).

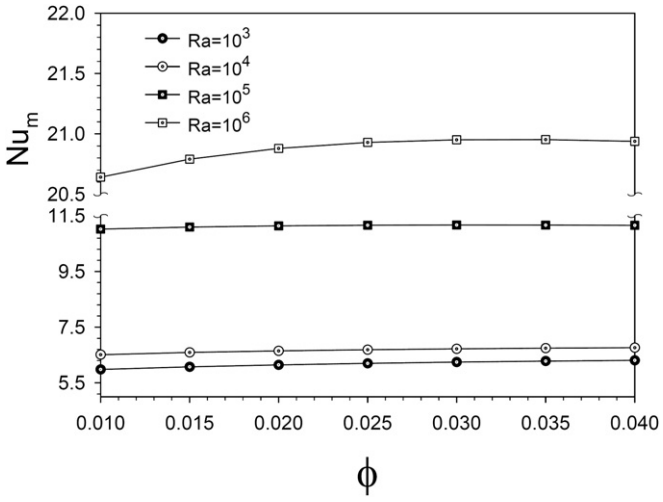

Fig. 6. Variation of average Nusselt with solid volume fraction at different Rayleigh numbers.

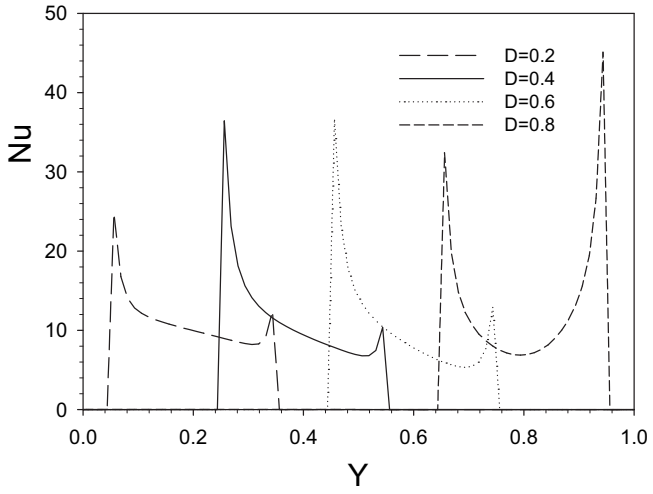

Fig. 8. Local Nusselt number along the heat source for different locations of the heat source.

This means that the buoyant flow becomes stronger and the heat transfer is enhanced at high Rayleigh numbers. Fig. 5c and d depict the variation of x-velocity (U) and temperature (θ), respectively, at $X = 0.5$ and for different Rayleigh numbers. It can be seen that as the Rayleigh number increases, the absolute magnitude of x-velocity increases indicating a stronger buoyant flow within the enclosure. The temperature profile at $X = 0.5$ shows a uniform increase in the temperature from the cold wall towards the bottom wall of the enclosure at $Ra = 10^3$ where the heat transfer is due to conduction. However, at high Rayleigh numbers, where convection dominates the heat transfer, the temperature reaches its maximum at a certain point along the $X = 0.5$ axis. Moreover, the magnitude of maximum temperature increases as Rayleigh number increases.

The analysis of heat transfer from the enclosure is carried out by examining the variation of the average Nusselt number along the heat source (Nu_m). Fig. 6 demonstrates the variation of Nu_m with respect to the solid volume fraction (ϕ) for different Rayleigh numbers ($10^3 \leq Ra \leq 10^6$). Firstly, it can be seen that the rate of heat transfer increases as the Rayleigh number increases. As mentioned earlier, this is due to the strengthening of the convection flow field at higher Rayleigh numbers. Secondly, at low Rayleigh numbers, where the heat transfer is mainly due to conduction, a continuous increase in the heat transfer rate is evident as the solid volume fraction increases. However, at high Rayleigh numbers, an optimum solid volume fraction is found, which results in the maximum heat transfer rate. This variation in the heat transfer rate highlights the importance of the solid volume fraction in the analysis of the heat transfer performance of the enclosure, which is also reported in the literature [34].

6.2. Heat source location

For this part of the analysis, an enclosure with AR = 1 and a nanofluid with $\phi = 0.04$ are considered. Rayleigh number varies in the range of $10^3 \leq Ra \leq 10^6$ and the distance of the heat source from the bottom wall of the enclosure varies in the range of $0.2 \leq D \leq 0.8$.

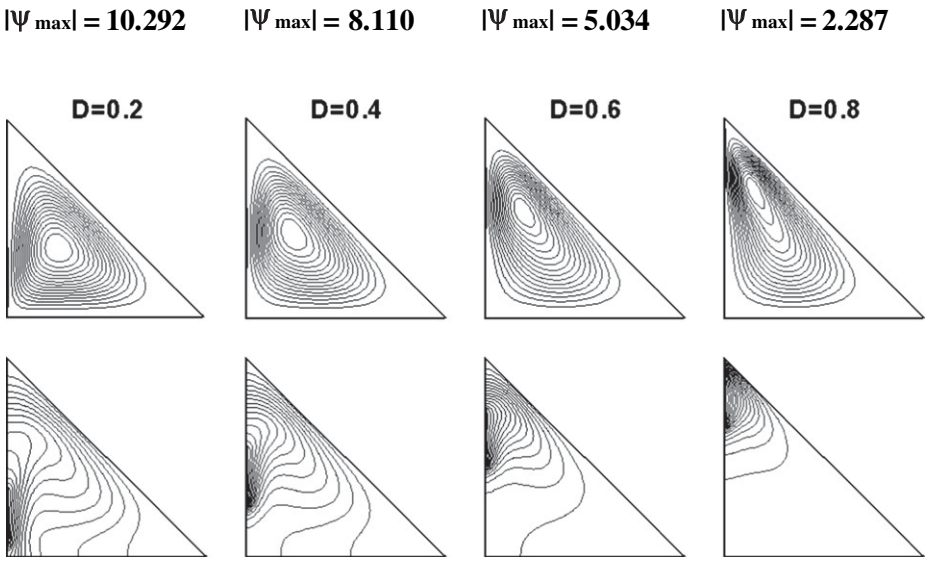

Fig. 7. Streamlines (top) and isotherms (bottom) for different heat source locations ($\phi = 0.04$ and $Ra = 10^5$).

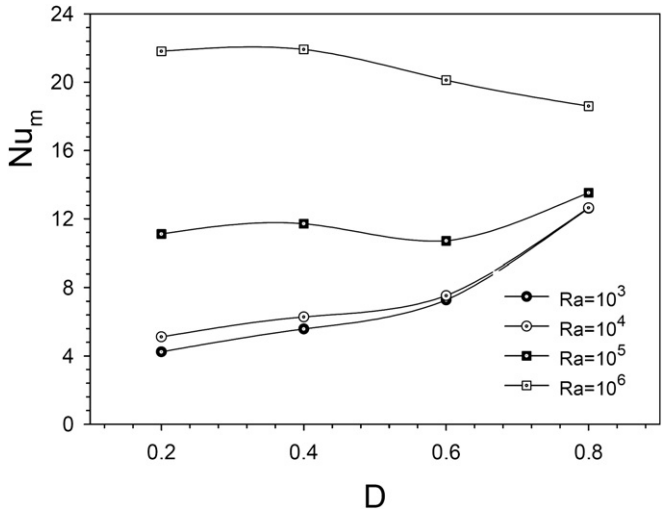

Fig. 9. Variation of average Nusselt number with the location of the heat source at different Rayleigh numbers.

Fig. 7 shows the streamlines (top) and the isotherms (bottom) for $Ra = 10^5$ and with different heat source locations. For all heat source locations, a single clock-wise circulation cell is observed within the enclosure. As the heat source moves upwards, the absolute magnitude of the stream function decreases and the isotherms are stratified near the top corner of the enclosure. This means weaker buoyant flow circulation is occurring in the enclosure, which suggests a lower heat transfer rate. On the other hand, it is noted that depending on Rayleigh number, the heat transfer is also expected to increase as the heat source moves upwards and approaches the cold wall.

In order to clarify this point and to develop a better understanding of the heat transfer performance of the enclosure, the heat transfer rate in terms of Nusselt number is studied. Fig. 8 demonstrates the profiles of the local Nusselt number along the heat source for different heat source locations. The results show different profiles for the local Nusselt number depending on the location of the heat source. However, for all locations, a sharp variation in the Nusselt number is observed near the edges of the heat source. This is because the heat transfer rate increases from zero on the thermally insulated left wall to a maximum value at the edge of the heat source. Fig. 9 clearly shows that at low Rayleigh numbers, where the heat transfer is mainly due to conduction, Nu_m increases as the heat source moves upwards (i.e. the distance between the heat source and the cold wall decreases). However, at high Rayleigh numbers ($Ra = 10^6$), where convection dominates the flow field, the convection circulation cell becomes weaker and consequently, the heat transfer rate decreases as the heat source moves upwards.

6.3. Enclosure aspect ratio

For this part of the analysis, the heat source is assumed to be located in the centre of the left wall ($D = 0.5$). The effect of

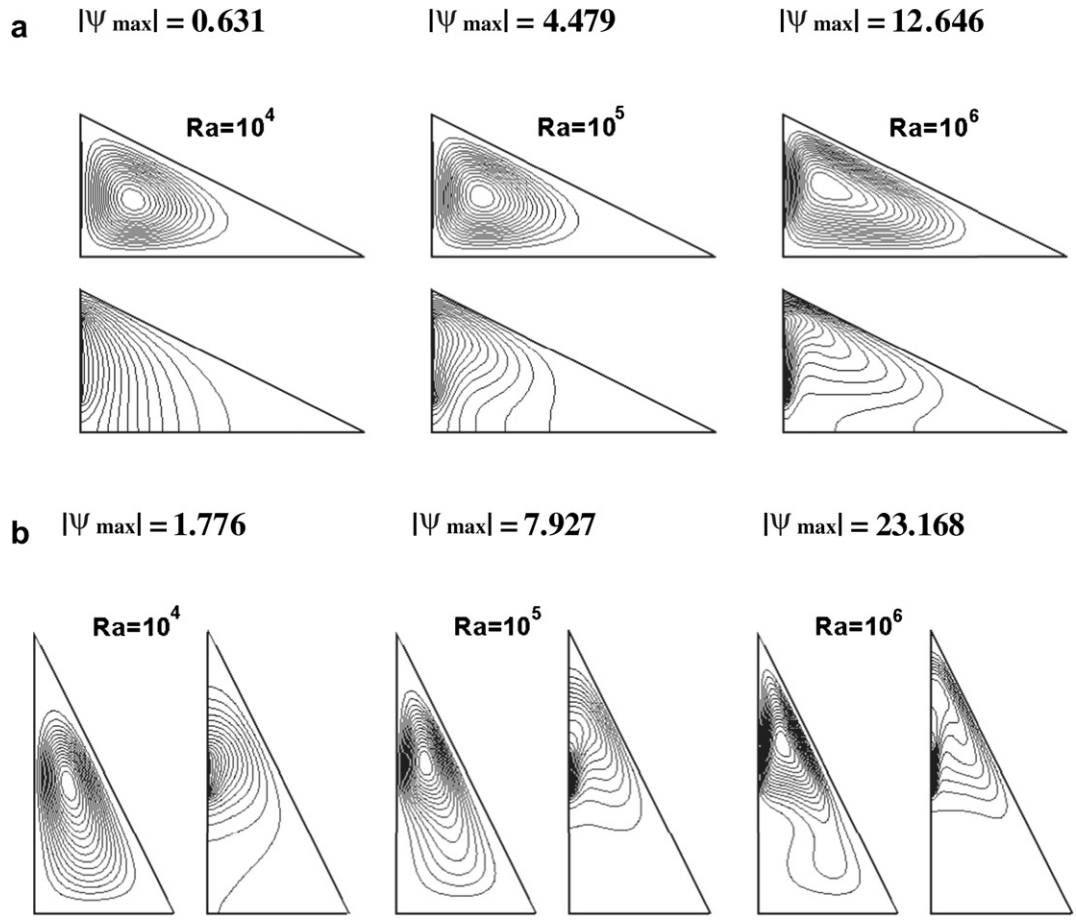

Fig. 10. a: Streamlines (top) and isotherms (bottom) at different Rayleigh numbers (AR = 0.5 and $\phi = 0.04$). b: Streamlines (left) and isotherms (right) at different Rayleigh numbers (AR = 2 and $\phi = 0.04$).

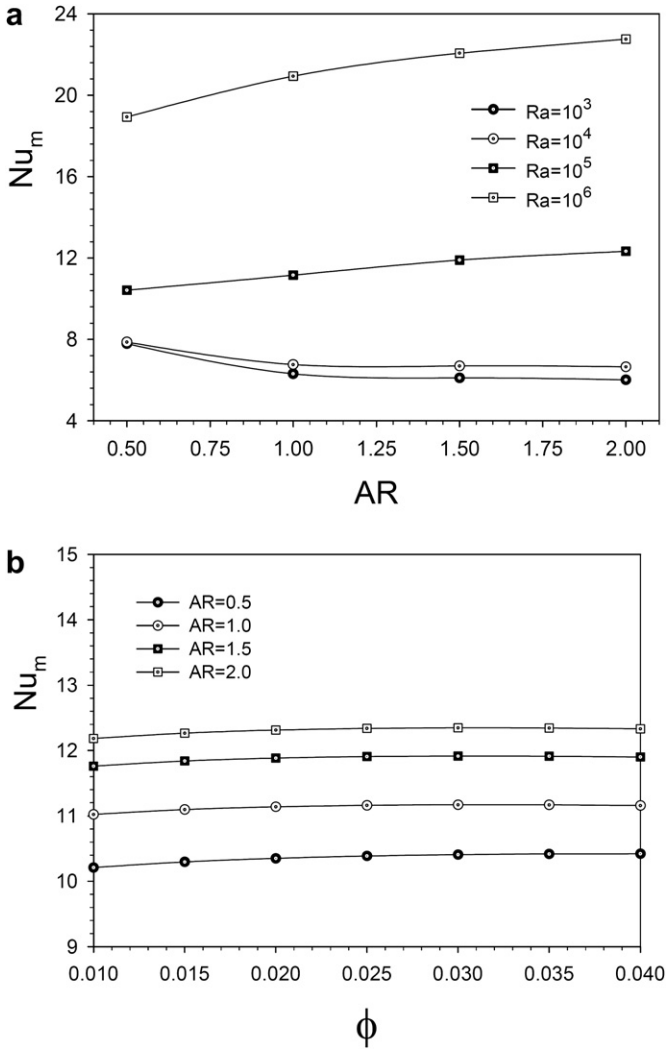

Fig. 11. a: Variation of average Nusselt number with enclosure aspect ratio at different Rayleigh numbers ($\phi = 0.04$). b: Variation of average Nusselt number with solid volume fraction at different enclosure aspect ratios ($Ra = 10^5$).

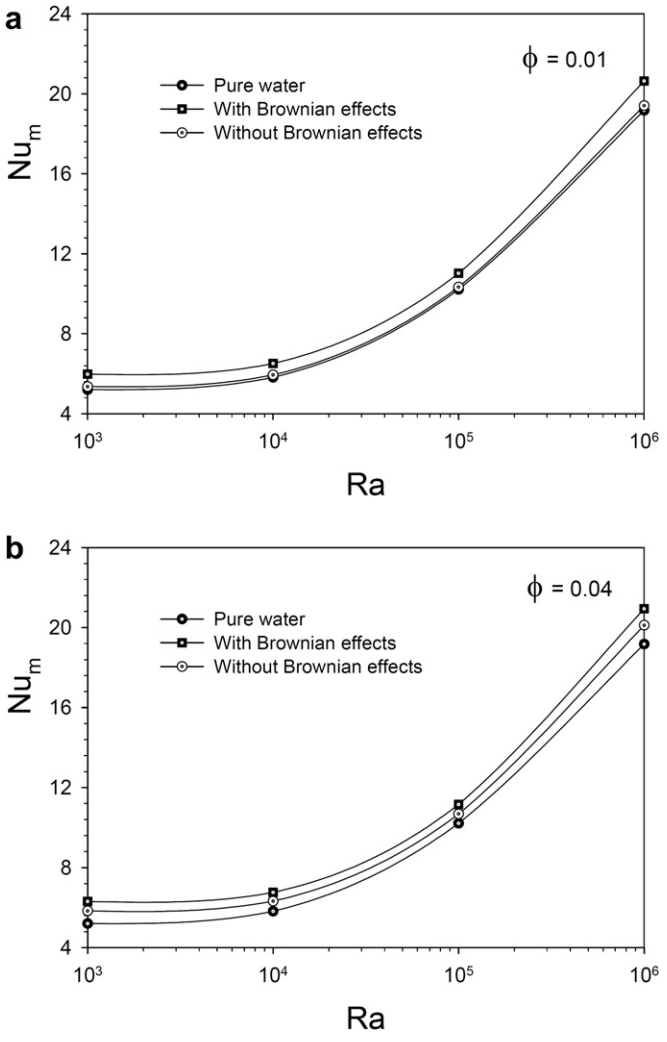

Fig. 12. a: The effects of Brownian motion on average Nusselt number ($\phi = 0.01$). b: The effects of Brownian motion on average Nusselt number ($\phi = 0.04$).

enclosure aspect ratio is investigated for the AR value range of $0.5 \leq AR \leq 2$. This is achieved by maintaining the length of horizontal wall (L) constant and varying the length of vertical wall of the enclosure (H).

Fig. 10a and b show the streamlines and isotherms for AR = 0.5 and AR = 2, respectively, and for a range of Rayleigh numbers from 10^4 to 10^6. The nanofluid with $\phi = 0.04$ is considered. It must be noted that the results for $Ra = 10^3$ are not presented as they are similar to the results for $Ra = 10^4$. A single, regular and relatively weak circulation cell is observed within the enclosure at $Ra = 10^4$ and for both aspect ratios. As the Rayleigh number increases, the circulation becomes irregular and stronger. For each Rayleigh number, as the aspect ratio increases from AR = 0.5 to AR = 2, the absolute value of stream function increases. An increase in AR means an increase in the length of the vertical wall while the length of the heat source is kept constant. Fig. 11a demonstrates that at low Rayleigh numbers, where conduction dominates the heat transfer, as AR increases the conduction heat transfer becomes weaker and therefore Nu_m decreases. Fig. 11b, however, shows that at high Rayleigh numbers ($Ra = 10^5$), where convection dominates the heat transfer, an increase of AR results in a stronger buoyant flow and consequently a higher heat transfer at any value of solid volume fraction.

6.4. Brownian motion

For this part of the analysis, the heat source is located in the centre of the vertical wall ($D = 0.5$) and the AR value is one. Two scenarios are considered: The first scenario includes Brownian motion and uses $\mu_{eff} = \mu_{Static} + \mu_{Brownian}$ and $k_{eff} = k_{Static} + k_{Brownian}$ as previously considered in the analysis. The second scenario neglects Brownian motion and uses $\mu_{eff} = \mu_{Static}$ and $k_{eff} = k_{Static}$. Fig. 12a and b show that for two different solid volume fractions ($\phi = 0.01$ and 0.04), the values of Nu_m are generally higher when Brownian motion is considered. Table 4 presents a comparison study for the increase in the average Nusselt number for the nanofluid with respect to pure water at various Rayleigh numbers ($10^3 \leq Ra \leq 10^6$) and solid volume fractions ($0 \leq \phi \leq 0.04$). The influence of ϕ on the Nu_m is more significant at low Rayleigh numbers for both models with and without Brownian motion. For example, at $Ra = 10^3$, for the nanofluid with $\phi = 0.04$, Nu_m increases by 21.2% with Brownian motion and by 12.1% without Brownian motion.

This section examines the variation of the ratio of the nanofluid average Nusselt number to the pure fluid average Nusselt number ($Nu_{m,nf}/Nu_{m,f}$) with respect to the solid volume fraction ($0.01 \leq \phi \leq 0.04$) for a range of Rayleigh numbers ($10^3 \leq Ra \leq 10^6$). The results considering Brownian motion are presented in Fig. 13a

Table 4
The Brownian motion effects on Nu_m at various Ra and ϕ ($D = 0.5, AR = 1$).

		$\phi = 0$	$\phi = 0.01$	$\phi = 0.02$	$\phi = 0.03$	$\phi = 0.04$
$Ra = 10^3$	$Nu_{m,Brownian}$	5.206	5.981	6.146	6.245	6.309
	Increase (%)	0	14.9	18.1	20.0	21.2
	$Nu_{m,Non-Brownian}$	5.206	5.359	5.515	5.674	5.836
	Increase (%)	0	2.9	5.9	9.0	12.1
$Ra = 10^4$	$Nu_{m,Brownian}$	5.823	6.513	6.649	6.723	6.764
	Increase (%)	0	11.9	14.2	15.5	16.2
	$Nu_{m,Non-Brownian}$	5.823	5.944	6.069	6.198	6.331
	Increase (%)	0	2.1	4.2	6.4	8.7
$Ra = 10^5$	$Nu_{m,Brownian}$	10.216	11.023	11.139	11.171	11.159
	Increase (%)	0	7.9	9.0	9.4	9.2
	$Nu_{m,Non-Brownian}$	10.216	10.336	10.453	10.569	10.684
	Increase (%)	0	1.2	2.3	3.5	4.6
$Ra = 10^6$	$Nu_{m,Brownian}$	19.171	20.641	20.879	20.951	20.938
	Increase (%)	0	7.7	8.9	9.3	9.2
	$Nu_{m,Non-Brownian}$	19.171	19.409	19.646	19.881	20.114
	Increase (%)	0	1.2	2.5	3.7	4.9

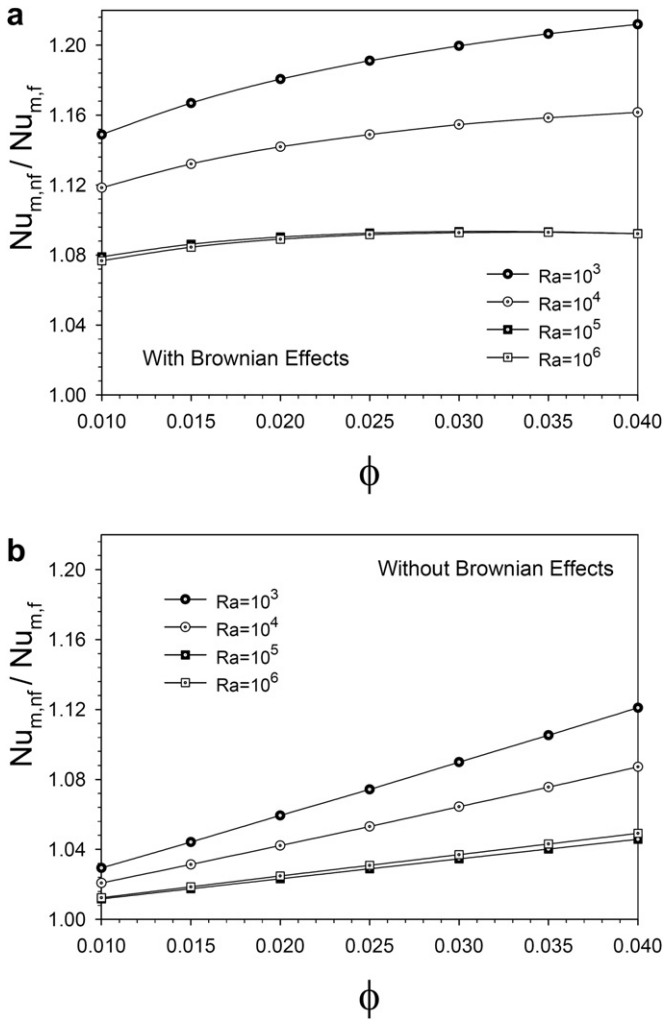

Fig. 13. a: Variation of average Nusselt number ratio with solid volume fraction at different Rayleigh numbers ($\mu_{nf} = \mu_{Static} + \mu_{Brownian}$ and $k_{eff} = k_{Static} + k_{Brownian}$). b: Variation of average Nusselt number ratio with solid volume fraction at different Rayleigh numbers ($\mu_{nf} = \mu_{Static}$ and $k_{eff} = k_{Static}$).

and the results not considering Brownian motion are presented in Fig. 13b. A comparison between Fig. 13a and b indicates that when Brownian motion is neglected, for all Rayleigh numbers, $Nu_{m,nf}/Nu_{m,f}$ continuously increases as ϕ increases. However, when Brownian motion is considered, at high Rayleigh numbers, an optimum value for ϕ can be found which results in the maximum $Nu_{m,nf}/Nu_{m,f}$.

7. Conclusions

Natural convection in a right triangular enclosure, with a heat source on its vertical wall and filled with a water–CuO nanofluid has been studied numerically. The effect of parameters such as the Rayleigh number, solid volume fraction, heat source location, enclosure aspect ratio and Brownian motion on the flow and temperature fields, as well as the heat transfer rate are examined. The results of the numerical analysis lead to the following conclusions.

For all values of the solid volume fraction, increasing the Rayleigh number results in a higher heat transfer rate due to strengthening of the buoyancy forces.

The location of the heat source proved to affect the heat transfer rate differently at various Rayleigh numbers. At low Rayleigh numbers, as the heat source moves upwards on the vertical wall of the enclosure, a higher heat transfer rate is achieved. However, at high Rayleigh numbers, particularly at $Ra = 10^6$, the opposite behaviour is observed.

The aspect ratio of the enclosure also affects the heat transfer rate differently at various Rayleigh numbers. In fact, an increase in the height of enclosure results in a lower heat transfer rate at low Rayleigh numbers and a higher heat transfer rate at high Rayleigh numbers.

A comparison between the two studies of with and without Brownian motion shows that when Brownian motion is considered, the solid volume fraction has dissimilar effects on the heat transfer rate at different Rayleigh numbers. At low Rayleigh numbers, a continuous increase in the heat transfer rate with respect to an increase in the solid volume fraction is found, whereas, at high Rayleigh umbers, an optimum solid volume fraction can be found, which results in the maximum heat transfer rate. When Brownian motion is neglected, the heat transfer rate continuously increases with the solid volume fraction at all Rayleigh numbers.

References

[1] V.A. Akinsete, T.A. Coleman, Heat transfer by steady laminar free convection in triangular enclosures. International Journal of Heat and Mass Transfer 25 (7) (1982) 991–998.

[2] H. Asan, L. Namli, Laminar natural convection in a pitched roof of triangular cross-section: summer day boundary conditions. Energy and Buildings 33 (1) (2000) 69–73.

[3] A. Omri, J. Orfi, S.B. Nasrallah, Natural convection effects in solar stills. Desalination 183 (1–3) (2005) 173–178.

[4] S.C. Kaushik, R. Kumar, H.P. Garg, J. Prakash, Transient analysis of a triangular built-in-storage solar water heater under winter conditions. Heat Recovery Systems and CHP 14 (4) (1994) 337–341.

[5] A. Ecevit, A.M. Al-Shariah, E.D. Apaydin, Triangular built-in-storage solar water heater. Solar Energy 42 (3) (1989) 253–265.

[6] K.A. Joudi, I.A. Hussein, A.A. Farhan, Computational model for a prism shaped storage solar collector with a right triangular cross section. Energy Conversion and Management 45 (3) (2004) 391–409.

[7] E.H. Ridouane, A. Campo, Heightened thermal convection as a result of splitting a square cavity diagonally in half. Journal of Electronic Packaging, Transactions of the ASME 128 (3) (2006) 251–258.

[8] E.H. Ridouane, A. Campo, J.Y. Chang, Natural convection patterns in right-angled triangular cavities with heated vertical sides and cooled hypotenuses. Journal of Heat Transfer 127 (10) (2005) 1181–1186.

[9] R.D. Flack, T.T. Konopnicki, J.H. Rooke, The measurement of natural convective heat transfer in triangular enclosures. Journal of Heat Transfer 101 (4) (1979) 648–654.

[10] D. Poulikakos, A. Bejan, Fluid dynamics of an attic space. Journal of Fluid Mechanics 131 (1983) 251–269.

[11] Y.E. Karyakin, Y.A. Sokovishin, O.G. Martynenko, Transient natural convection in triangular enclosures. International Journal of Heat and Mass Transfer 31 (9) (1988) 1759–1766.

[12] E. Martin del Campo, M. Sen, E. Ramos, Analysis of laminar natural convection in a triangular enclosure. Numerical Heat Transfer 13 (3) (1988) 353–372.

[13] E. Fuad Kent, E. Asmaz, S. Ozerbay, Laminar natural convection in right triangular enclosures. Heat and Mass Transfer/Waerme- und Stoffuebertragung 44 (2) (2007) 187–200.

[14] E.H. Ridouane, A. Campo, Effects of attaching baffles onto the inclined walls of attic frames for purposes of energy conservation. Heat Transfer Engineering 28 (2) (2007) 103–111.

[15] Y. Varol, A. Koca, H.F. Oztop, Natural convection heat transfer in Gambrel roofs. Building and Environment 42 (3) (2007) 1291–1297.

[16] R.D. Flack, K. Brun, R.J. Schnipke, Measurement and prediction of natural convection velocities in triangular enclosures. International Journal of Heat and Fluid Flow 16 (2) (1995) 106–113.

[17] S.U.S. Choi, Enhancing thermal conductivity of fluids with nanoparticles. ASME Fluids Engineering Division 231 (1995) 99–105.

[18] N. Putra, W. Roetzel, S.K. Das, Natural convection of nano-fluids. Heat and Mass Transfer 39 (8–9) (2003) 775–784.

[19] D. Wen, Y. Ding, Formulation of nanofluids for natural convective heat transfer applications. International Journal of Heat and Fluid Flow 26 (6) (2005) 855–864.

[20] C.J. Ho, M.W. Chen, Z.W. Li, Numerical simulation of natural convection of nanofluid in a square enclosure: effects due to uncertainties of viscosity and thermal conductivity. International Journal of Heat and Mass Transfer 51 (17–18) (2008) 4506–4516.

[21] E. Abu-Nada, Effects of variable viscosity and thermal conductivity of Al_2O_3–water nanofluid on heat transfer enhancement in natural convection. International Journal of Heat and Fluid Flow 30 (4) (2009) 679–690.

[22] S.P. Jang, S.U.S. Choi, Role of Brownian motion in the enhanced thermal conductivity of nanofluids. Applied Physics Letters 84 (21) (2004) 4316–4318.

[23] Y. Xuan, Q. Li, W. Hu, Aggregation structure and thermal conductivity of nanofluids. AIChE Journal 49 (4) (2003) 1038–1043.

[24] D.H. Kumar, H.E. Patel, V.R.R. Kumar, T. Sundararajan, T. Pradeep, S.K. Das, Model for heat conduction in nanofluids. Physical Review Letters 93 (14) (2004) 144301.

[25] J. Koo, C. Kleinstreuer, A new thermal conductivity model for nanofluids. Journal of Nanoparticle Research 6 (6) (2004) 577–588.

[26] R. Prasher, P. Bhattacharya, P.E. Phelan, Thermal conductivity of nanoscale colloidal solutions (nanofluids). Physical Review Letters 94 (2) (2005) 1–4.

[27] S.M.S. Murshed, K.C. Leong, C. Yang, A combined model for the effective thermal conductivity of nanofluids. Applied Thermal Engineering 29 (11–12) (2009) 2477–2483.

[28] J.C. Maxwell, A Treatise on Electricity and Magnetism, vol. II, Oxford University Press, Cambridge, UK, 1873, pp. 54.

[29] R.L. Hamilton, O.K. Crosser, Thermal conductivity of heterogeneous two-component systems. Industrial and Engineering Chemistry Fundamentals 1 (3) (1962) 187–191.

[30] S.V. Patankar, Numerical Heat Transfer and Fluid Flow. Hemisphere Publishing Corporation, Taylor and Francis Group, New York, 1980, pp. 113–137.

[31] Y. Varol, H.F. Oztop, A. Koca, Entropy production due to free convection in partially heated isosceles triangular enclosures. Applied Thermal Engineering 28 (2008) 1502–1513.

[32] S.C. Tzeng, J.H. Liou, R.Y. Jou, Numerical simulation-aided parametric analysis of natural convection in a roof of triangular enclosures. Heat Transfer Engineering 26 (8) (2005) 69–79.

[33] H.F. Oztop, E. Abu-Nada, Numerical study of natural convection in partially heated rectangular enclosures filled with nanofluids. International Journal of Heat and Fluid Flow 29 (5) (2008) 1326–1336.

[34] B. Ghasemi, S.M. Aminossadati, Natural convection heat transfer in an inclined enclosure filled with a water–CuO nanofluid. Numerical Heat Transfer, Part A: Applications 55 (8) (2009) 807–823.

[35] Y. Hwang, J.K. Lee, C.H. Lee, Y.M. Jung, S.I. Cheong, C.G. Lee, B.C. Ku, S.P. Jang, Stability and thermal conductivity characteristics of nanofluids. Thermochimica Acta 455 (1–2) (2007) 70–74.

[36] H.C. Brinkman, The viscosity of concentrated suspensions and solution. Journal of Chemical and Physics 20 (1952) 571–581.

[37] J. Koo, C. Kleinstreuer, Laminar nanofluid in microheat-sinks. International Journal of Heat and Mass Transfer 48 (13) (2005) 2652–2661.

[38] S. Palm, G. Roy, C.T. Nguyen, Heat transfer enhancement with the use of nanofluids in a radial flow cooling system considering temperature dependent properties. Applied Thermal Engineering 26 (2006) 2209–2218.

[39] A. Akbarinia, A. Behzadmehr, Numerical study of laminar mixed convection of a nanofluid in horizontal curved tubes. Applied Thermal Engineering 27 (2007) 1327–1337.